Journal of The Electrochemical
Society

The Electrochemical Society
Advancing solid state & electrochemical science & technology

Mechano-Electrochemical Analysis in Cylindrical Composition-Gradient Electrodes with Varying Young's Modulus of Lithium-Ion Battery

To cite this article: Hanzhong Xing *et al* 2019 *J. Electrochem. Soc.* **166** A762

Journal of The Electrochemical Society, **166** (4) A762-A770 (2019)
0013-4651/2019/166(4)/A762/9/$38.00 © The Electrochemical Society

Mechano-Electrochemical Analysis in Cylindrical Composition-Gradient Electrodes with Varying Young's Modulus of Lithium-Ion Battery

Hanzhong Xing,[1] Yulan Liu,[1,z] and B. Wang[2,z]

[1]*School of Aeronautics and Astronautics, Sun Yat-Sen University, Guangzhou 510275, People's Republic of China*
[2]*School of Physics, Sun Yat-Sen University, Guangzhou 510275, People's Republic of China*

Composition-gradient electrode material (CGEM) is one of the most promising materials in lithium-ion battery, and this paper studies its performance from the stress analysis. The finite deformation theory and the stress-induced diffusion hypothesis are adopted to establish the constitutive equations, and the nonlinear influence of finite deformation is considered. The aim is to investigate diffusion-induced stresses (DISs) generated in a cylindrical composition-gradient electrode with the slope of -0.5 for Young's modulus E(R). Compared with stress distributions in a homogeneous electrode, CGEM is able to make the stress fields smaller and flatter and improve the state of charging (SOC). Then we change the elastic modulus of electrode materials from 10GPa to 150GPa gradually, and those advantages still exist. Finally, diffusion-induced buckling of cylindrical electrodes is analyzed and CGEMs make the cylindrical electrode more difficult to buckle. Therefore, many electrode materials can be made into CGEMs to prevent the electrode from cracking. The results can provide a theoretical guidance for the design of CGEMs.

[DOI: 10.1149/2.1031904jes]

Manuscript submitted October 29, 2018; revised manuscript received February 11, 2019. Published March 8, 2019.

The lithium-ion battery is one of the most promising secondary cells. In recent years, it has been the stored-energy apparatus of many portable electronic devices and electric vehicles due to its long cycle life, high-energy capacity, low self-discharge rate, high open circuit voltage and its environmental friendly merit.[1,2] From a mechanical point of view, lithium-ion batteries have their own weaknesses. During charging and discharging, the volume of electrodes will change with the lithiation and delithiation. As anode materials, silicon has the highest Li-ion intercalation capacity (4200mAh/g) which is about ten times of that of graphite materials.[3,4] But a silicon anode will generate about 400 percent of volume deformation in the electrode when the electrode is completely lithiated. Such large volume deformation will leads to large strain energy. The accumulation of strain energy may make the silicon electrode crack or degrade electrochemically.[5–7] As cathode materials commonly used now, $LiCoO_2$ cathodes can generate large stresses when it is constrained, and these stresses may fracture electrodes.[8]

Excessive stresses in electrode are the main reason that make the electrode failure. The stresses produced by deformation that can crack the electrode are called diffusion-induced stresses (DISs). Therefore, sufficient analysis of DISs can enable us to better protect the electrode. Prussin started the initial research of DISs in silicon wafer.[9] Since then, more and more researchers have shown great interest in the study of DISs in various compositional solids. Zhang[10] investigated DISs in layered Li-ion battery electrode plates. They found that the material of current collector should be as soft and flexible as possible to reduce DISs. Yang et al.[11] analyzed the DISs caused by insertion deformation in a spherical electrode particle under potentiostatic and galvanostatic conditions. Rutooj Deshpande et al.[12] investigated DISs in nanowire electrode structures under plane strain condition and generalized plane strain condition. Song et al.[13] worked out the analytical solutions of DISs in a cylindrical multilayer electrode and provided many design insights for LIBs. Li et al.[14] considered the dislocation effect on diffusion-induced stress in electrodes and also got the analytical expressions of DISs. Zhang et al.[15] studied the effect of reversible electrochemical reaction on DISs and diffusion in a cylindrical electrode. They compared solutions of reaction induced stress with that of diffusion induced stresses in electrodes and got that the former is larger. Christensen and Newman[16] and Zhang[17] introduced the chemical potential coupling for diffusion and stresses. Woodford et al.[18] studied the electrochemical shock of intercalation electrodes and analyzed the fracture mechanics failure in electrode particles. Pallab Barai et al.[19] developed a stochastic computational methodology to capture the large deformation and mechanical degradation in high-capacity anode materials.

The studies above all used the linear elastic theory to analyze DISs and ignored nonlinear influence of large deformation. Many other scholars have made achievements in these fields. Zhao et al.[20] formulated a large plastic deformation theory based on nonequilibrium thermodynamics. They mainly studied the effect of plastic yielding on the magnitude of DISs in silicon electrodes. Cui et al.[21] introduced the development of a new stress-dependent chemical potential for solid-state diffusion under multiple driving forces in tensor form and investigated the influence of plastic deformation in electrodes.

Recently many researchers studied other factors that affect the stresses of the electrode and how to reduce these stresses. Li et al.[22] studied the influence of local velocity on diffusion-induced stress in large-deformation electrodes and they found that this influence could negligible for the immobile boundary condition. Duan et al.[23] investigated a coupled electrochemical–thermal–mechanical model for spiral-wound Li-ion batteries. Weng et al.[24] analyzed DISs in their own negative Poisson's ratio electrode under different operations. It provides a new idea for the selection of electrode materials.

This paper focuses on the material itself. So many studies are looking for the substitution and improving the preparation technology in LIB anode materials. Among advanced materials substituted for $LiCoO_2$, composition-gradient materials shows better electrochemical performances in many ways.[25,26] We focuses on stress analysis of composition-gradient materials under different conditions. Compared to those above single homogeneous materials, the studies have synthesized two kinds of new-style composition-gradient materials as spherical electrode particle, which are $LiMn_{1.87}Ni_{0.13}O_4$ and $Li_{1.2}(Mn_{0.62}Ni_{0.38})_{0.8}O_2$.[27,28] The concentration of Ni increases and that of Mn of the former material decreases from the core to the surface and the latter material has an opposite trend. Both of them have excellent characteristics in the electrochemical performance. The composition-gradient electrode $LiMn_{1.87}Ni_{0.13}O_4$ has a capacity retention of 90.2% after 200 cycles, while the $LiMn_2O_4$ was only 57.8% in the same test conditions. Moreover, the capacity of the composition-gradient electrode $Li_{1.2}(Mn_{0.62}Ni_{0.38})_{0.8}O_2$ retained 97% after 100 cycles relative to the first cycle at a rate of C/2. However, a few of literatures focus on the mechanical and electrochemical properties about these new composition-gradient materials. It is difficult to obtain themechanical and electrochemical properties of these two composition-gradient electrodes.

The main work of this paper is to study the difference between composition-gradient electrodes and homogeneous electrodes in cylindrical shape. We try to use the mechanical and electrochemical parameters of $LiMn_2O_4$ as the properties of homogeneous electrodes.

---

[z]E-mail: stslyl@mail.sysu.edu.cn; wangbiao@mail.sysu.edu.cn

The compositions of the composition-gradient material vary continuously from the center to the surface. Therefore, we assume that the composition-gradient electrodes are homogeneous electrodes whose properties change continuously from the electrode center to its surface. Besides, we focus on the elastic modulus. We just change the elastic modulus, and we treat the material that changes the modulus of elasticity as different materials. Then we get how gradient influence on the different of DISs, SOC and axial force that produce in inhomogeneous and homogeneous electrodes at various elastic modulus. In addition, we consider the nonlinear influence of large deformation and the interaction between diffusion and stresses. We choose nonlinear finite deformation theory mainly because it contains nonlinear terms. When the higher order quantities are ignored, the nonlinear finite deformation theory can be reduced to the linear elastic small deformation theory. So our model is more general because it involves nonlinear deformation. After this, composition-gradient materials will be extended to a wider range of materials and provide a theoretical guidance for the design of composition-gradient electrode materials.

Basic Theory

Mechanical equilibrium.—The electrode may generate large volume deformation when lithium-ions diffuse into or out of the electrode. To better describe the problem, there are two descriptions which are Lagrangian form and Eulerian form. Lagrangian form is based on the initial configuration, while Eulerian form is based on the current configuration. In the cylindrical electrode with an initial radius of R_0, the coordinate system in the Lagrangian description is (R, Θ, Z). And the corresponding coordinate system in the Eulerian description is (r, θ, z) after a period of time t. Based on the above definition, the total deformation gradient tensor in the cylindrical coordinate is defined as

$$\mathbf{F} = \begin{bmatrix} F_{11} & & \\ & F_{22} & \\ & & F_{33} \end{bmatrix} = \begin{bmatrix} 1+\frac{\partial u}{\partial R} & & \\ & 1+\frac{u}{R} & \\ & & 1+\frac{\partial w}{\partial Z} \end{bmatrix}, \qquad [1]$$

where u is the radial displacement, and w is the axial displacement. The total deformation $\mathbf{F}$ includes elastic part $\mathbf{F}^e$ and inelastic part $\mathbf{F}^i$. Here, the plasticity of the composition-gradient electrode is not considered.

$$\mathbf{F} = \mathbf{F}^e\,\mathbf{F}^{\mathrm{i}}. \qquad [2]$$

Lithium-ions diffusion causes the inelastic volume expansion, so it is assumed to be isotropic. So the inelastic deformation gradient tensor is adopted as follow.[29]

$$\mathbf{F}^i = (\Lambda^i)^{\frac{1}{3}}\mathbf{I}, \qquad [3]$$

where $\mathbf{I}$ is the unit tensor and Λ^i is the inelastic volume ratio. The inelastic volume ratio is dominated by the lithium-ion concentration C based on the Lagrangian description. So it is expressed as

$$\Lambda^i = 1+\Omega\mathrm{C}, \qquad [4]$$

where Ω is the diffusion partial molar volume.

The components of the elastic deformation gradient tensor $\mathbf{F}^e$ is given as

$$\mathbf{F}^e = \mathbf{F}\left(\mathbf{F}^i\right)^{-1} = \begin{bmatrix} \left(1+\frac{\partial u}{\partial R}\right)\left(\Lambda^i\right)^{-\frac{1}{3}} & & \\ & \left(1+\frac{u}{R}\right)\left(\Lambda^i\right)^{-\frac{1}{3}} & \\ & & \left(1+\frac{\partial w}{\partial Z}\right)\left(\Lambda^i\right)^{-\frac{1}{3}} \end{bmatrix}, \qquad [5]$$

The total Green-Lagrange strain tensor $\mathbf{E}$ can be written as

$$\mathbf{E} = \frac{1}{2}\left(\mathbf{F}^{\mathrm{T}}\mathbf{F}\text{-}\mathbf{I}\right), \qquad [6]$$

Combined with Eq. 2, the elastic Green-Lagrange strain tensor $\mathbf{E}^e$ and the inelastic Green-Lagrange strain tensor $\mathbf{E}^i$ can be expressed as

$$\mathbf{E}^e = \frac{1}{2}\left((\mathbf{F}^{\mathrm{e}})^{\mathrm{T}}\mathbf{F}^{\mathrm{e}}\text{-}\mathbf{I}\right), \qquad [7]$$

$$\mathbf{E}^i = \frac{1}{2}\left((\mathbf{F}^{i})^{\mathrm{T}}\mathbf{F}^{i}\text{-}\mathbf{I}\right), \qquad [8]$$

where $\mathbf{I}$ is the second order unit matrix.

Then we need to get the stresses of the electrode. The non-zero components of the first Piola-Kirchhoff stress $\boldsymbol{\sigma}^0$ can be determined by

$$\boldsymbol{\sigma}^0 = \frac{\partial W}{\partial \mathbf{F}} = \frac{\partial W}{\partial \mathbf{E}^{\mathrm{e}}}\frac{\partial \mathbf{E}^{\mathrm{e}}}{\partial \mathbf{F}^{\mathrm{e}}}\frac{\partial \mathbf{F}^{\mathrm{e}}}{\partial \mathbf{F}}, \qquad [9]$$

where W is the elastic strain energy density. It is assumed as a function of Green–Lagrange strain tensor[21,30]

$$W = \Lambda^i\frac{\mathrm{E}}{2(1+\upsilon)}\left\{\frac{\upsilon}{1-\upsilon}[tr\,(\mathbf{E}^e)]^2 + tr\,(\mathbf{E}^e\mathbf{E}^e)\right\}, \qquad [10]$$

where E and υ are the Young's modulus and Poisson's ratio of the composition-gradient electrode, respectively.

Substituting Eqs. 4 and 10 into Eq. 9, we can obtain

$$\boldsymbol{\sigma}^0 = \Lambda^i\frac{\mathrm{E}}{2(1+\upsilon)}\left[\frac{2\upsilon}{1-2\upsilon}tr\,(\mathbf{E}^e) + 2\mathbf{E}^e\right]\frac{\mathbf{F}^e}{\mathbf{F}^i}, \qquad [11]$$

Combining Eqs. 1, 3, 4, 5 and 7 with Eq. 11 leads to

$$\sigma_R^0 = (1+\Omega\mathrm{C})\frac{\mathrm{E}}{(1+\upsilon)(1-2\upsilon)} \times \left[(1-\upsilon)\mathrm{E}_R^e + \upsilon\left(\mathrm{E}_\Theta^e + \mathrm{E}_Z^e\right)\right]\frac{2\mathrm{E}_R^e+1}{1+\frac{\partial u}{\partial R}}, \qquad [12]$$

$$\sigma_\Theta^0 = (1+\Omega\mathrm{C})\frac{\mathrm{E}}{(1+\upsilon)(1-2\upsilon)} \times \left[(1-\upsilon)\mathrm{E}_\Theta^e + \upsilon\left(\mathrm{E}_R^e + \mathrm{E}_Z^e\right)\right]\frac{2\mathrm{E}_\Theta^e+1}{1+\frac{u}{R}}, \qquad [13]$$

$$\sigma_Z^0 = (1+\Omega\mathrm{C})\frac{\mathrm{E}}{(1+\upsilon)(1-2\upsilon)} \times \left[(1-\upsilon)\mathrm{E}_Z^e + \upsilon\left(\mathrm{E}_\Theta^e + \mathrm{E}_R^e\right)\right]\frac{2\mathrm{E}_Z^e+1}{1+\frac{\partial w}{\partial Z}}, \qquad [14]$$

where σ_R^0, σ_Θ^0 and σ_Z^0 are components of the first Piola-Kirchhoff stress $\boldsymbol{\sigma}^0$. E_{R}^e, E_Θ^e and E_Z^e are components of the elastic Green-Lagrange strain tensor $\mathbf{E}^e$ given as

$$\mathrm{E}_R^e = \frac{1}{2}\left[\frac{\left(1+\frac{\partial u}{\partial R}\right)^2}{(1+\Omega\mathrm{C})^{\frac{2}{3}}} - 1\right], \qquad [15]$$

$$\mathrm{E}_\Theta^e = \frac{1}{2}\left[\frac{\left(1+\frac{u}{R}\right)^2}{(1+\Omega\mathrm{C})^{\frac{2}{3}}} - 1\right], \qquad [16]$$

$$\mathrm{E}_Z^e = \frac{1}{2}\left[\frac{\left(1+\frac{\partial w}{\partial Z}\right)^2}{(1+\Omega\mathrm{C})^{\frac{2}{3}}} - 1\right], \qquad [17]$$

The velocity of atomic diffusion is much slower than that of elastic deformation, so the quasi-static mechanical equilibrium is assumed.[31] Then, in the absence of body force, the equations of mechanical equilibrium in the cylindrical coordinate are

$$\frac{\partial \sigma_R^0}{\partial R} + \frac{\sigma_R^0 - \sigma_\Theta^0}{R} = 0, \qquad [18]$$

$$\frac{\partial \sigma_Z^0}{\partial Z} = 0. \tag{19}$$

The mechanical equilibrium behavior is governed by Eqs. 12∼19.

Diffusion equation.—According to the law of mass conservation, the diffusion kinetic equation in the Lagrangian description should be expressed as

$$\frac{\partial C}{\partial t} + \frac{\partial (RJ)}{R \partial R} = 0, \tag{20}$$

where C is the concentration of lithium-ions in the Lagrangian description. J is the radial diffusion flux of the solute based on the Lagrangian description. Moreover, the true concentration of lithium-ions c in the Eulerian description is related to C and can be expressed as follow

$$C = c \cdot det(\mathbf{F}) = c F_R F_\Theta F_Z, \tag{21}$$

where F_R, F_Θ and F_Z are components of the total deformation gradient tensor $\mathbf{F}$

The true diffusion flux j in the Eulerian description is a function of the chemical potential μ.

$$j = -\frac{cD}{R_g T} \frac{\partial \mu (r, c)}{\partial r}, \tag{22}$$

where D is the diffusivity of Lithium-ions in the electrode, R_g is the gas constant and T is the temperature. Combining Eq. 21 with Eq. 22, the diffusion flux J in the Lagrangian description can be written as

$$J = -\frac{CD}{R_g T} \frac{1}{{F_R}^2} \frac{\partial \mu (R, C)}{\partial R}, \tag{23}$$

where $\mu(R, C)$ is expressed by the Lagrangian coordinates.

Considering many factors, the form of the chemical potential per mole can be expressed as[32]

$$\mu (r, c) = \mu_0 + R_g T log(\gamma c) - \Omega \sigma_m + \Omega w, \tag{24}$$

where $\mu(r, c)$ is the chemical potential based on the Euler description, μ_0 is a reference value, γ is the activity coefficient and σ_m is the hydrostatic stress. Here, we let γ equal to 1. w being the strain energy density in the Eulerian description. The strain energy density represents the deformation energy stored on the surface of the solid due to elastic deformation introduced by the electromechanical interaction and surface perturbations. It expressed as

$$w = \frac{W}{\det(\mathbf{F}^i)} = \frac{\mathrm{E}}{2(1+\upsilon)} \left\{ \frac{\upsilon}{1-\upsilon} [\mathrm{tr}\,(\mathbf{E}^e)]^2 + \mathrm{tr}\,(\mathbf{E}^e \mathbf{E}^e) \right\}, \tag{25}$$

From Eqs. 21∼23, we can obtain

$$J = j F_\Theta F_Z. \tag{26}$$

Substituting Eq. 24 into Eq. 22 and combining Eq. 26, the diffusion flux J is formulated as

$$\begin{aligned} J = {} & -\mathrm{D} \frac{\mathrm{F}_\Theta \mathrm{F}_Z}{\mathrm{F}_R} \frac{\partial}{\partial R} \left(\frac{\mathrm{C}}{\mathrm{F}_R \mathrm{F}_\Theta \mathrm{F}_Z} \right) \\ & + \frac{1}{R_g T} \frac{\mathrm{CD}}{{\mathrm{F}_R}^2} \left(\frac{\partial \Omega}{\partial R} \sigma_m + \frac{\partial \sigma_\mathrm{m}}{\partial R} \Omega - \frac{\partial \Omega}{\partial R} w - \frac{\partial w}{\partial R} \Omega \right), \end{aligned} \tag{27}$$

where the diffusion partial molar volume Ω could be a function of the radial coordinate R in the Lagrangian description. And the hydrostatic stress σ_m is expressed as

$$\sigma_m = \frac{1}{3} (\sigma_R + \sigma_\Theta + \sigma_Z), \tag{28}$$

while the first Piola-Kirchhoff stress $\boldsymbol{\sigma}^0$ and the Cauchy stress $\boldsymbol{\sigma}$ have a relationship as follow

$$\boldsymbol{\sigma}^0 = det(\mathbf{F}) \boldsymbol{f} \boldsymbol{\sigma} \tag{29}$$

in which $\boldsymbol{f} = \frac{\partial \mathbf{X}}{\partial \mathbf{x}} = \mathbf{I} - \frac{\partial \mathbf{u}}{\partial \mathbf{x}}$

Therefore, the Cauchy stress $\boldsymbol{\sigma}$ can be denoted by the first Piola-Kirchhoff stress $\boldsymbol{\sigma}^0$ as

$$\begin{aligned} \sigma = \langle \sigma_R, \sigma_\Theta, \sigma_Z \rangle = \Bigg\langle & \frac{1}{\left(1 + \frac{u}{R}\right)\left(1 + \frac{\partial w}{\partial Z}\right)} \sigma_R^0, \ \frac{1}{\left(1 + \frac{\partial u}{\partial R}\right)\left(1 + \frac{\partial w}{\partial Z}\right)} \sigma_\Theta^0, \\ & \frac{1}{\left(1 + \frac{\partial u}{\partial R}\right)\left(1 + \frac{u}{R}\right)} \sigma_Z^0 \Bigg\rangle. \end{aligned} \tag{30}$$

The diffusion kinetic behavior is dominated by Eqs. 20, 27 and 30.

In a cylindrical composition-gradient electrode, the material properties vary along the radial direction. However, these properties remain the same along the azimuthal and the axial direction. Therefore, the elastic modulus E is the functions of radial coordinate E(R) in the Lagrangian description.

Boundary and initial conditions.—We assume that the radial surface of the cylinder is stress-free and the cylindrical center has no displacement, that is

$$\sigma_R^0 (R_0, t) = 0, \tag{31}$$

$$u(0, t) = 0, \tag{32}$$

Potentiostatic operation is set to a constant concentration C_{max} at the surface, that is the formula

$$C(R_0, t) = C_{max}, \tag{33}$$

while the boundary conditions for galvanostatic operation are given by

$$J(R_0,\ t) = \frac{i_n}{\mathrm{F}}, \tag{34}$$

where i_n is the applied current density and F is the Faraday's constant.

At the center of the cylinder, the diffusion flux J is given as

$$J(0,\ t) = 0, \tag{35}$$

Constraints are imposed on the top and bottom faces of the cylinder to constrain the deformation of the ends in the axial direction. We assume that such constraints may not prevent the ends of the cylinder from moving in the lateral direction, that is w = 0 on the faces of the ends.

At last, we adopt Li-free, stress-free and displacement-free initial conditions in the cylinder, that is

$$C(R,\ 0) = 0, \tag{36}$$

$$u(R,\ 0) = 0. \tag{37}$$

Results and Discussion

It's almost impossible to get the analytical solution of equations above, so we solve numerically the system of equations described in Basic Theory section by using the finite element method (COMSOL Multiphysics). As mentioned in previous papers, it is difficult to obtain the mechanical and electrochemical properties of the composition-gradient electrodes. The exact functions of $E(R)$ have not been fully understood and studied. Following the previous assumption,[29] these functions are linear with several different slopes of radial coordinate R. Once the properties are constant along the radial coordinate, the inhomogeneous theory in Basic Theory section reduces to the theory in a homogeneous cylindrical particle of $LiMn_2O_4$. It is assumed that E(R) is simple linear functions of R given as follow

$$\mathrm{E}(R) = k_1 \left(\frac{R}{R_0} - \frac{1}{2} \right) E_0 + E_0 \tag{38}$$

where k_1 is respectively dimensionless slopes of the Young's modulus. One previous paper has drawn the conclusion that the optimal slope

Table I. Material properties and operating parameters of $LiMn_2O_4$.[29]

Parameter	Symbol	Value
Young's modulus	E_0	$10GPa$
Poisson's ratio	υ	0.3
Surface lithium-ion concentration	C_{max}	$2.29 \times 10^4\ mol\ m^{-3}$
Diffusion partial molar volume	Ω_0	$3.497 \times 10^{-6}\ m^3\ mol^{-1}$
Gas constant	R_g	$8.31\ \mathrm{J}\ mol^{-1}\ K^{-1}$
Diffusion coefficient	D_0	$7.08 \times 10^{-15}\ m^2\ s^{-1}$
Temperature	T	$273\ K$
Faraday's constant	F	$96485.3365\ A\ s\ mol^{-1}$
Cylinder radius	R_0	$2.25 \times 10^{-6}\ m$

for inhomogeneous E(R) is −0.5 for $LiMn_2O_4$ which elastic modulus is 10GPa,[31] so in our paper k_1 is −0.5. According to our research, D(R) only influences the velocity of diffusion. It has little influence on stresses. And this paper mainly considers the influence of elastic modulus, so the results of D(R) are not listed.

The main purpose for this paper is study the effect of gradient on DISs of different materials in a cylindrical composition-gradient electrode during potentiostatic operation. Here we only focus on the elastic modulus, so we use the material properties and operating parameters of $LiMn_2O_4$ and only change the elastic module from 10GPa to 150GPa gradually. By this assumption, different materials with different elastic modulus are represented. Then we get how gradient influence on them. The material properties of $LiMn_2O_4$ are listed in Table I,[29] which will be also used as reference values in a cylindrical composition-gradient electrode.

Here, the state of charging (SOC), is used to represent the percentage of full capacity and to evaluate the charging process of the cylinder. This is also an important research content of this paper. Thus, SOC is given as[31]

$$\mathrm{SOC} = \frac{\int_0^{R_0} CR\,dR}{\int_0^{R_0} C_{steady-state} R\,dR}, \qquad [39]$$

And the normalized time τ is represented as

$$\tau = Dt/R^2, \qquad [40]$$

The elastic modulus E_0 we choose 10GPa, 50GPa, 100GPa, 150GPa. These four values basically represent the range of elastic modulus of the electrode material from low to high. Moreover previous papers that studied the $LiMn_2O_4$ have selected 10GPa, 40GPa and 190 GPa[29,34] as its elastic modulus values.

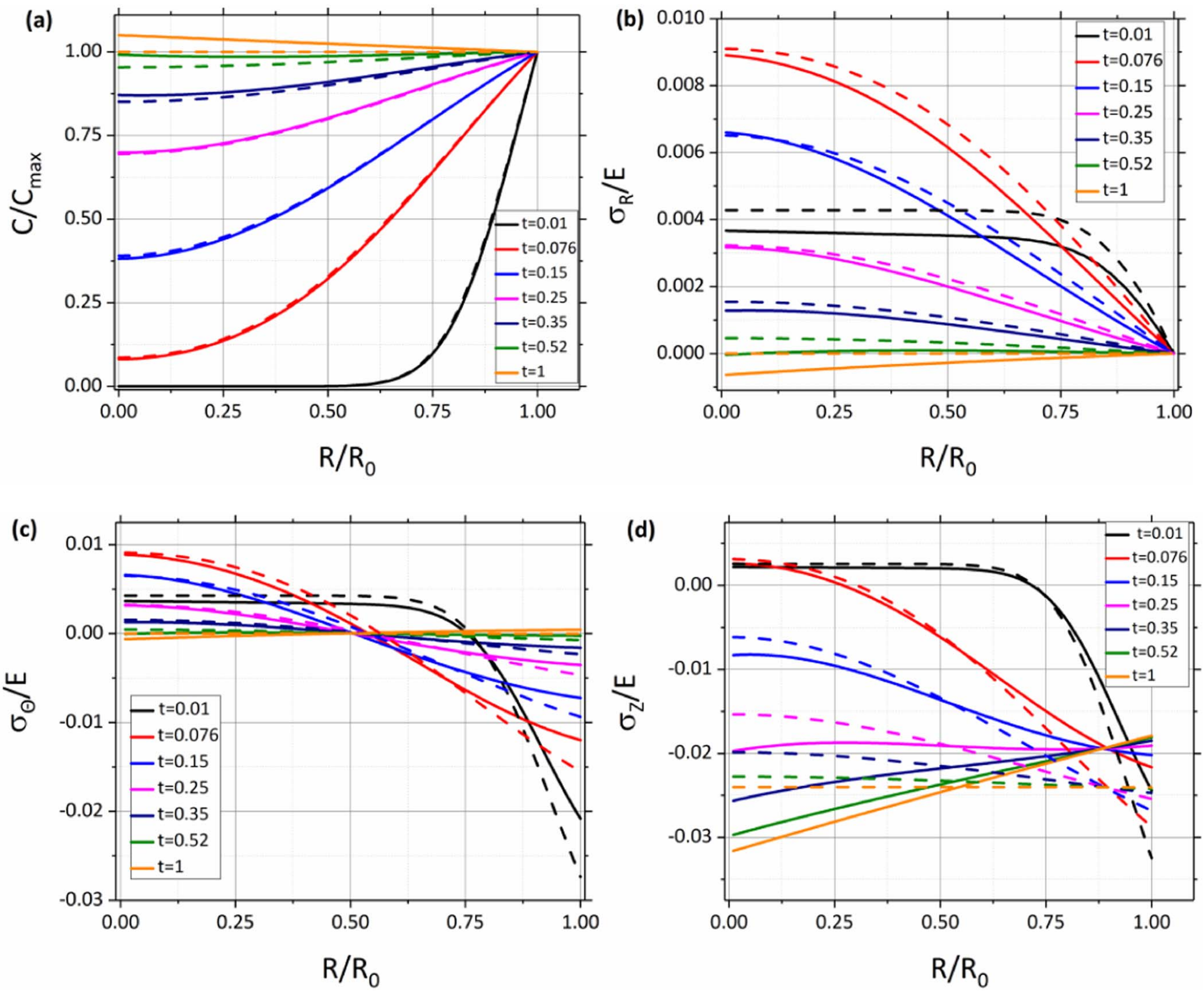

Figure 1. Illustrations of lithium-ion concentration (a), radial stress (b), hoop stress (c) and axial stress (d) of homogeneous and inhomogeneous of $E_0 = 10GPa$ at different normalized time.

Lithium-ion concentration and stress fields.—Solid lines plot the results of an inhomogeneous cylindrical particle, while dashed lines plot the results of a homogeneous cylindrical particle. In addition, if not specified, all results in this part follow this rule.

Fig. 1 illustrates lithium-ion concentration and stress fields for homogeneous and inhomogeneous elastic modulus E(R) of $E_0 = 10GPa$ at different normalized time. In Fig. 1a the influence of inhomogeneous elastic modulus E(R) is not obvious at most normalized times, but it can make the concentration at the center reach the maximum faster, which means it is easier to fill and has the higher charging efficiency. In addition, the lithium-ion concentration exceed the maximum concentration. This is mainly due to E(R). The hydrostatic stress σ_m at the steady-state is non-uniform pressure stress in the composition-gradient electrodes, while σ_m is non-uniform in the homogeneous electrodes. At the steady-state, the hydrostatic pressure is lower at the center and higher at the surface in the inhomogeneous electrodes. The existence of non-uniform hydrostatic pressure leads to the non-uniform chemical potential according to Eq. 24. Therefore, the distribution of concentration is non-uniform at the steady-state according to Eq. 27. The hydrostatic pressure can inhibit lithium-ion diffusion. Therefore, the lower hydrostatic pressure means the higher lithium-ion concentration. The boundary condition is that lithium-ion concentration is C_{max} at the surface. So the lithium-ion concentration exceed the maximum concentration at steady-state. In Fig. 1b, radial stress of inhomogeneous material is a little lower than that of homogeneous material, but it has a small value and is in the same direction along the radius, not the main stress that causes fracture. In Fig. 1c, negative gradient E(R) can effectively decrease the magnitudes at the surface of the electrode and reduce the positive hoop stress at the center, especially at the beginning. It is generally believed that the main reason leading to electrode materials fracture is hoop stress,[8,18,35,36] so negative gradient E(R) can prevent the electrode from cracking. In Fig. 1d, at the center of the electrode, inhomogeneous E(R) hardly affects the axial stress values at the beginning and then makes a great difference that gradient E(R) increases the magnitudes of axial stresses. Nevertheless, at the surface of the electrode, negative gradient E(R) can effectively decrease the magnitudes of axial stresses, especially at the beginning. In addition, the stress distributions, especially the axial stress, change unevenly along the coordinate R finally, while the stress distributions are flat in a homogeneous electrode at the same time. These results are consistent with the simulation results of References 31,33.

Fig. 2 illustrates lithium-ion concentration and stress fields for homogeneous and inhomogeneous elastic modulus E(R) of $E_0 = 50GPa$ at different normalized time. Similar to Fig. 1, the results are almost identical. In Fig. 2a the concentration will reach the maximum faster for inhomogeneous elastic modulus E(R), which means that it has the

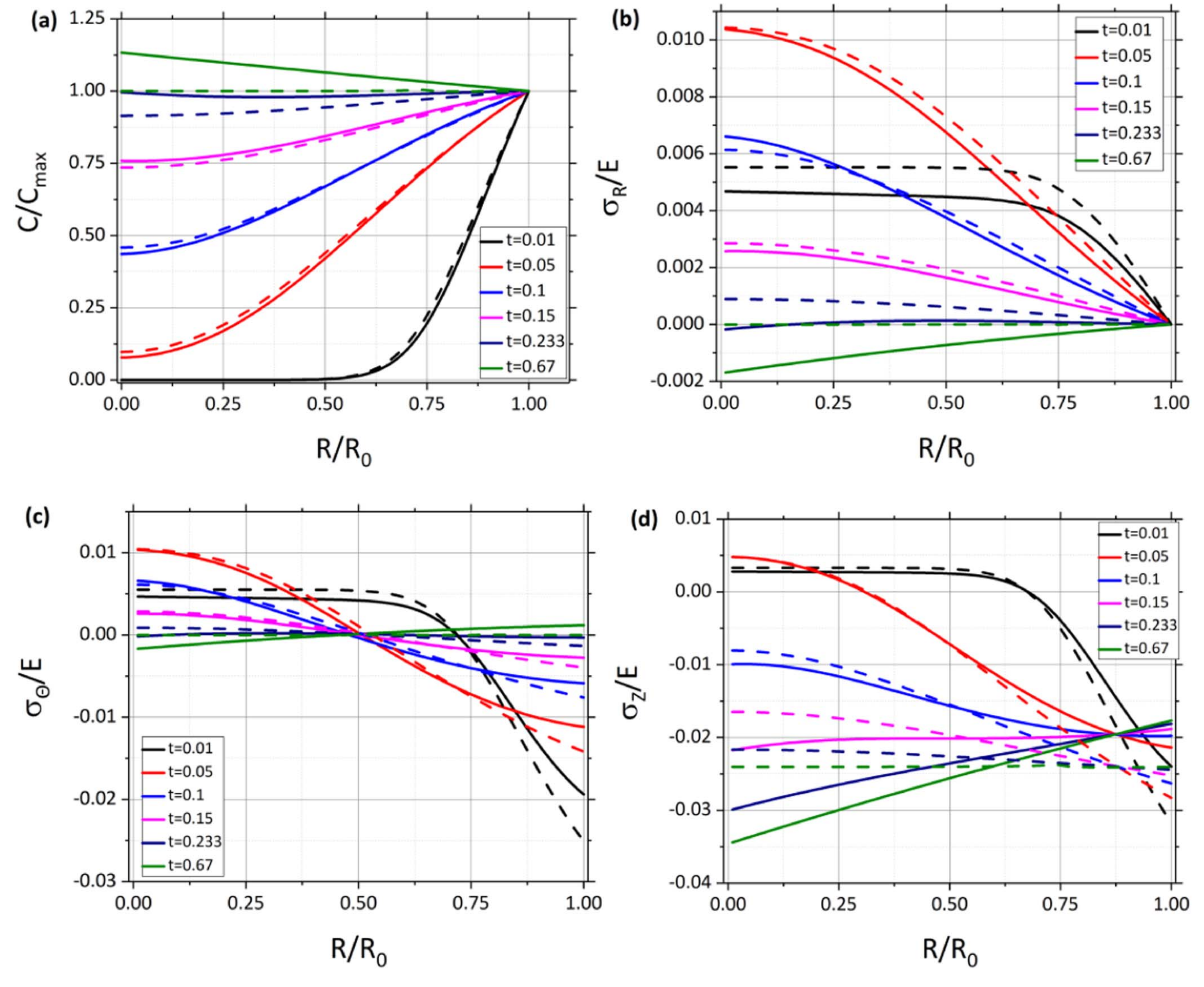

Figure 2. Illustrations of lithium-ion concentration (a), radial stress (b), hoop stress (c) and axial stress (d) of homogeneous and inhomogeneous of $E_0 = 50GPa$ at different normalized time.

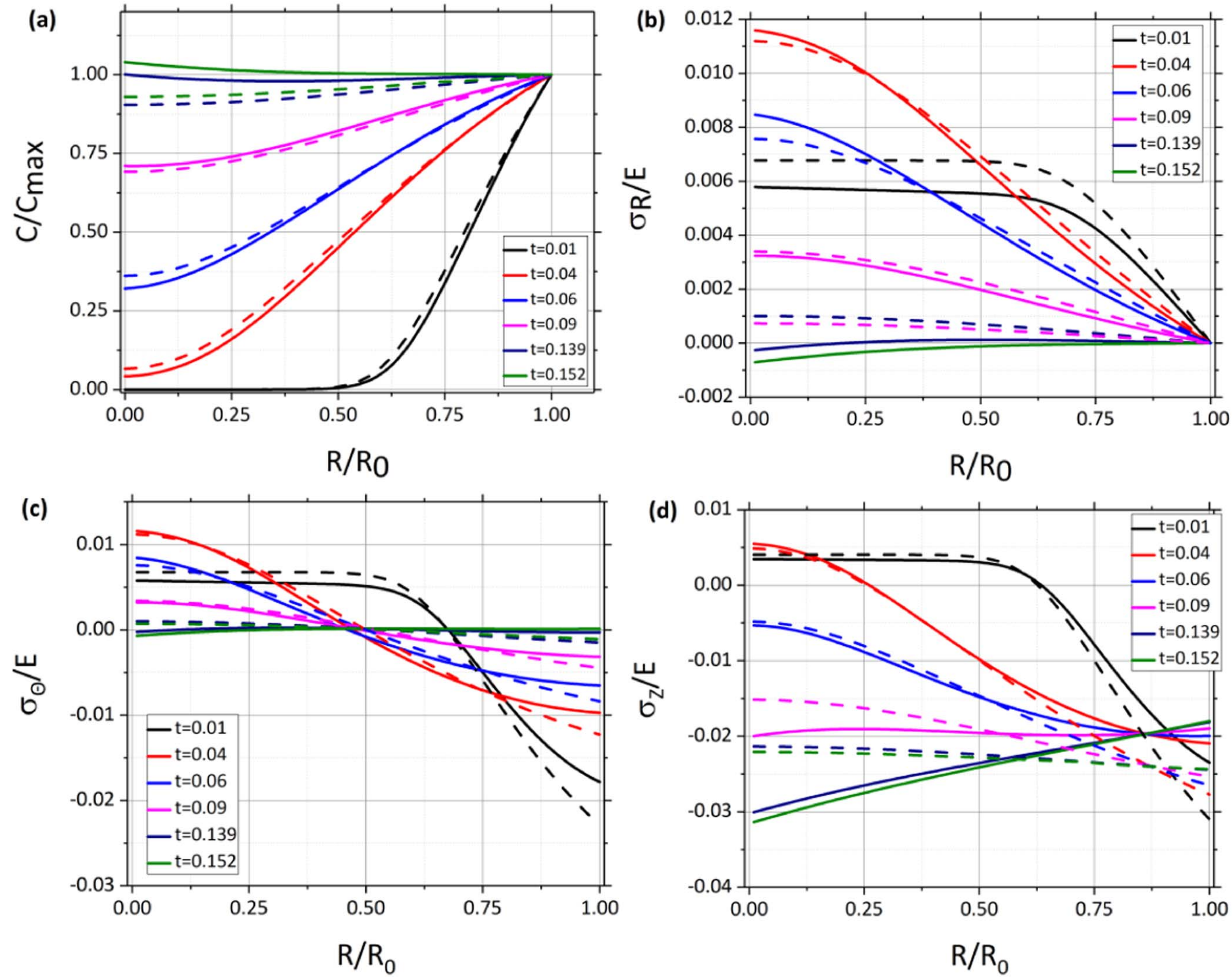

Figure 3. Illustrations of lithium-ion concentration (a), radial stress (b), hoop stress (c) and axial stress (d) of homogeneous and inhomogeneous of $E_0 = 100GPa$ at different normalized time.

higher charging efficiency. In Fig. 2b radial stress of inhomogeneous material is a little lower than that of homogeneous. In Fig. 2c, at the surface of the electrode, negative gradient E(R) can effectively decrease the magnitudes and the difference between center and surface of hoop stresses. So gradient E(R) can prevent the electrode damage. In Fig. 2d, at the center of the electrode, inhomogeneous E(R) make a great difference that gradient E(R) increases the magnitudes of axial stresses, but can effectively decrease the magnitudes of axial stresses at the electrode surface. However, there are still some differences, the concentration at the center of the electrode increases more and more rapidly, indicating that the larger the elastic modulus, the faster the charge will be.

Fig. 3 illustrates lithium-ion concentration and stress fields for homogeneous and inhomogeneous elastic modulus E(R) of $E_0 = 100GPa$ at different normalized time. The elastic modulus becomes large and the trend of the results in this case is similar to that in previous cases. In Fig. 3a, compared to the previous figures, the influence of inhomogeneous elastic modulus E(R) is more obvious, it makes the concentration at the center increase slower at the beginning and reach the maximum faster finally. However, we also can observe that the concentration at the center cannot reach the maximum for homogeneous material at the high elastic modulus E_0, while it can reach for the maximum inhomogeneous material. As for the results of the three stresses, they are same as before largely. In Fig. 3c, the inhomogeneous elastic modulus reduces the hoop stress and effectively prevents the electrode from cracking. However, with the increase of elastic modulus E_0, the maximum value of each stress also increases. It can be concluded that even with the increase of elastic modulus, inhomogeneous material can have a good protective effect on the electrode and can improve the percentage of full capacity.

Fig. 4 illustrates lithium-ion concentration and stress fields for homogeneous and inhomogeneous elastic modulus E(R) of $E_0 = 150GPa$ at different normalized time. The trend of the results in this case is similar to that in previous cases. In Fig. 4a, the influence of inhomogeneous elastic modulus E(R) makes the concentration at the center increase slower at the beginning and reaches the maximum faster finally. However, we can observe that the concentration at the center cannot reach the maximum for homogeneous material at the high E_0, and it can neither reach for the maximum inhomogeneous material. So we know that inhomogeneous elastic modulus E(R) can improve the percentage of full capacity while cannot reach the maximum due to the elastic modulus is too large. As for the results of the three stresses, they are same as before largely. In Fig. 4c, the inhomogeneous elastic modulus reduces the hoop stress and effectively prevents the electrode damage. However, with the increase of elastic modulus E_0, the maximum value of each stress also increases. In addition, different from when the elastic modulus is small, when the elastic modulus is

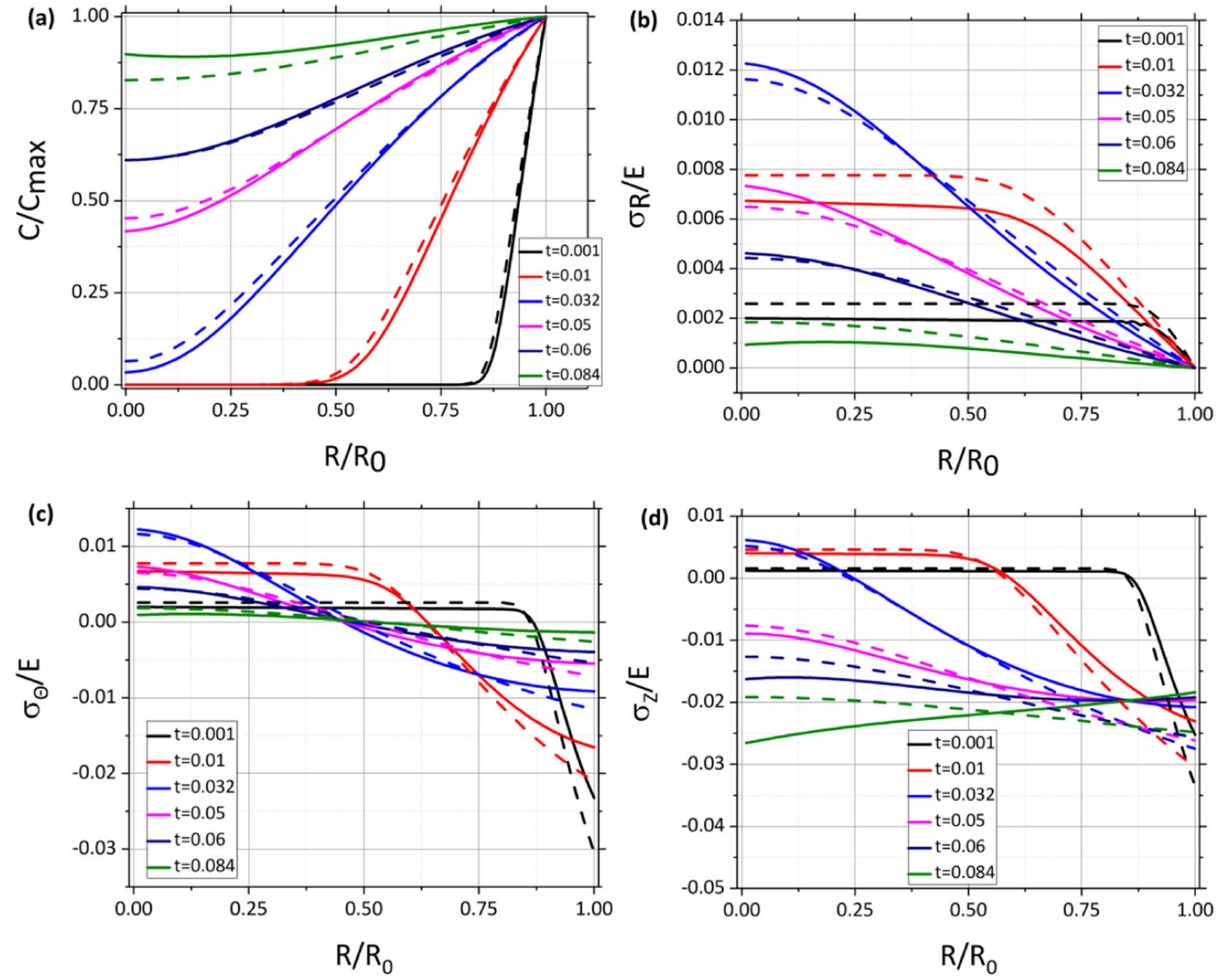

Figure 4. Illustrations of lithium-ion concentration (a), radial stress (b), hoop stress (c) and axial stress (d) of homogeneous and inhomogeneous of $E_0 = 150GPa$ at different normalized time.

high, the stress distributions change unevenly along the coordinate R finally in a homogeneous electrode, while the stress distributions are more even in an inhomogeneous electrode. It can be concluded that even with the increase of elastic modulus, inhomogeneous material can have a good protective effect on the electrode.

The state of charging (SOC).—In order to prove that the gradient material can improve the SOC of the electrode under various elastic modulus, the following results are obtained (here, we are considering the deformation of the electrode and do the correction), as shown in Fig. 5. Firstly, with the increase of elastic modulus, the charging time of the electrode is gradually shortened, and the maximum SOC of the electrode is gradually decreased. Secondly, under any elastic modulus, inhomogeneous materials can improve the final SOC of the electrode, but it is not obvious when the value of the elastic modulus is smaller than 10GPa and larger than 150GPa. Finally, we can also found that the value of SOC cannot be more than ninety percent when the elastic modulus is larger than 150GPa, even if we use the inhomogeneous

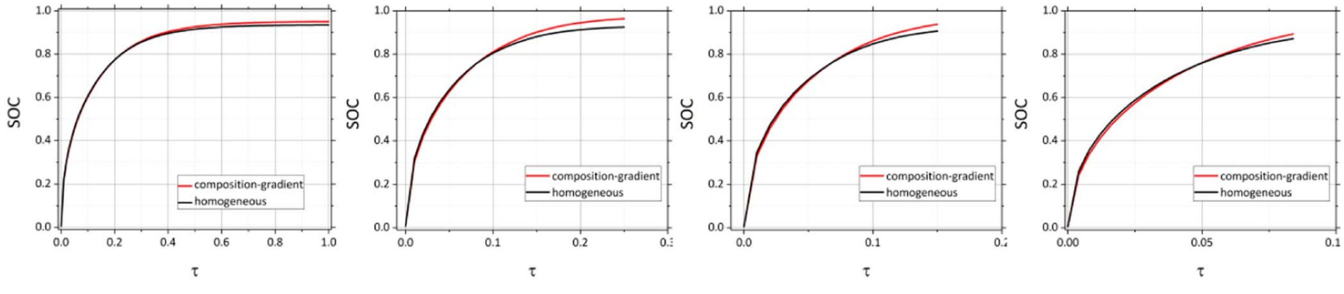

(a) E_0=10GPa (b) E_0=50GPa (d) E_0=100GPa (e) E_0=150GPa

Figure 5. Illustrations of SOC of homogeneous and inhomogeneous of each E_0 at different normalized time.

material as electrode. Therefore, the elastic modulus has a great influence on the storage capacity of the electrode.

Analysis of diffusion-induced buckling of cylindrical electrodes.—According to the results of the previous section, it can be seen that there is a great difference in the distribution of axial stress between composition-gradient materials and homogeneous materials. Here we consider the electrode particles as slender cylinders. In the mechanical, this is a plane strain problem. There are some papers considering that the constraint conditions of the cylindrical electrode is a free end and a fixed end. However, in the actual situation, the constraint conditions of the electrode is uncertain. The constraint condition might be that both ends of the electrode are fixed ends. When both ends of the cylinder electrode are fixed in axial direction, the axial force on both ends will be increased as the charging process goes on. When the axial force at both ends of a column of a certain length increases to the critical axial force of bending, the column will lose stability and undergo bending failure. It is necessary to study the effect of composition-gradient material on the buckling of cylindrical electrode.

The axial force on both ends of the cylinder is

$$F_Z = 2\pi \int_0^{R_0} \sigma_Z\, r\, dr, \qquad [41]$$

where σ_Z is the axial stress, it can be obtained from result at the condition of $E_0 = 10GPa$

In order to effectively judge the critical axial force of compression bending of slender cylinder, Euler bending criterion is selected here. The formula is

$$F_{crit} = \frac{\pi^2 EI}{(\chi L)^2}\,. \qquad [42]$$

Where F_{crit} is critical axial force that causes the column to bend. E is the elastic modulus of material and $E = 10GPa$. I is the moment of inertia of a cylindrical section

$$I = \frac{\pi R^4}{4}, \qquad [43]$$

and EI is the bending stiffness of the cylindrical electrode material. χ is the coefficient considering the constraint conditions at both ends. L is the length of the electrode and $L = 20R$.

The above bending criterion is for static pressure bending model, and this chapter develops the bending criterion to consider dynamic process. Therefore, it is assumed that the electrode charging process is a slow process, which ensures that the electrode is suitable for the improved bending criterion. In addition, the displacement in the radius of the electrode increases with time during the charging process. So the radius is modified as follow

$$R = R_0\left(1 + \frac{\partial u}{\partial r}\right). \qquad [44]$$

The charge state of the electrode *Capacity* is defined as follows

$$Capacity = \frac{2\pi \int_0^{R_0} Crdr}{2\pi \int_0^{R_0} rdr}\,. \qquad [45]$$

It represents the charging state of the electrode in the reference configuration.

In practice, the constraint conditions of both ends of the electrode is uncertain. Therefore, in order to better simulate electrode buckling under various conditions, three boundary conditions were selected. The first condition is that both ends of the electrode are pinned ends and it means $\chi = 1$. The second condition is that both ends of the electrode are a pinned end and a fixed end and it means $\chi = 0.7$. The third condition is that both ends of the electrode are fixed ends and it means $\chi = 0.5$. Under these conditions, a small disturbance will cause the cylinder to buckle when the axial force F_Z exceeds its critical stress F_{crit}. For the electrode, both the uneven doping of the material and the defects caused by the expansion of the electrode may cause small perturbations. Then the electrode particles will buckle. The result is shown in Fig. 6.

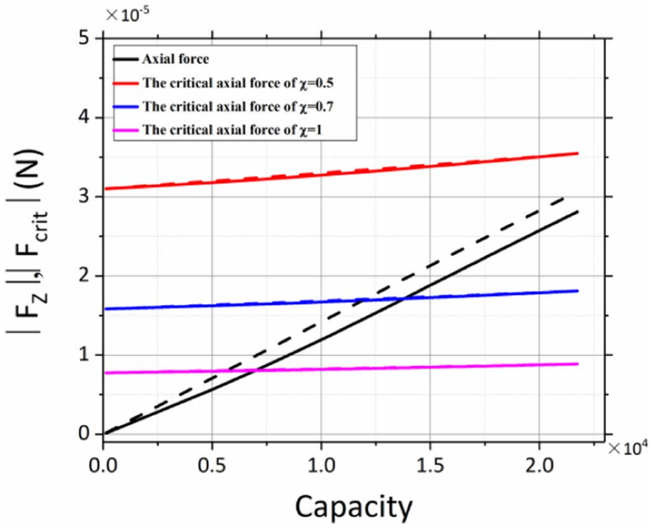

Figure 6. Illustrations of axial force and the critical force of the different constraint conditions of homogeneous and inhomogeneous at different capacity.

As shown in Fig. 6, the three nearly horizontal curves are in order from bottom to top: $\chi = 1$, $\chi = 0.7$ and $\chi = 0.5$. The axial force in the composite gradient material electrode is significantly smaller than that in the homogeneous material electrode at any Capacity. Therefore, the Capacity value of the intersection point of the axial force of composition-gradient material electrodes and three critical stress values is much larger than that of homogeneous material electrodes. The composition-gradient material can reduce the buckling of the electrode.

Conclusions

In this paper, we have formulated a theory in a cylindrical composition-gradient electrode constrained axially by considering the interaction effects of diffusion and stress. Combining with the diffusion theory and the finite deformation theory, the constitutive equations are established to analyze an electrode of being charged under potentiostatic operation. We have validated previous studies, the slope of -0.5 for E(R) from the electrode center to its surface are able to decrease the maximum stresses comparing with that in a homogeneous electrode and make stress distributions flatter. Therefore, the electrode can be well protected from being damaged by force during charging and discharging. Moreover, we can find that the center and the surface of an electrode are two critical positions where the maximum stresses are generated. Then we extended this study and found that under different elastic modulus, from 10GPa to 150GPa gradually. Negative gradient E(R) can also improve charging speed, reduce the maximum stress, and improve the state of charging (SOC). That is, from the point of stress analysis, the negative gradient may have a function improvement on many electrode materials. Many electrode materials can be made into composition-gradient electrode materials to prevent electrode from cracking, and the choice of the slope depends on the function and practical application of electrodes. Composition-gradient material can make the cylindrical electrode more difficult to buckle, thus better protecting the electrode. These theoretical results need to be tested experimentally in future. We hope that they provide some guidance on the design of composition-gradient electrodes.

Acknowledgments

We are grateful for support from National Science Foundation under grant No. 11572355 and grant No. 10572155.

ORCID

Hanzhong Xing https://orcid.org/0000-0002-2087-611X
Yulan Liu https://orcid.org/0000-0001-7253-3365

References

1. J. M. Tarascon and M. Armand, *Nature*, **414**, 359 (2001).
2. M. Armand and J. M. Tarascon, *Nature*, **451**, 652 (2008).
3. U. Kasavajjula, C. Wang, and A. J. Appleby, *Journal of Power Sources*, **163**, 1003 (2007).
4. W.-J. Zhang, *Journal of Power Sources*, **196**, 13 (2011).
5. L. Y. Beaulieu, K. W. Eberman, R. L. Turner, L. J. Krause, and J. R. Dahn, *Electrochemical and Solid-State Letters*, **4**, A137 (2001).
6. X. Xiao, P. Liu, M. W. Verbrugge, H. Haftbaradaran, and H. Gao, *Journal of Power Sources*, **196**, 1409 (2011).
7. S. W. Lee, M. T. McDowell, L. A. Berla, W. D. Nix, and Y. Cui, *Proceedings of the National Academy of Sciences of the United States of America*, **109**, 4080 (2012).
8. K. Zhao, M. Pharr, J. J. Vlassak, and Z. Suo, *Journal of Applied Physics*, **108**, 073517 (2010).
9. S. Prussin, *Journal of Applied Physics*, **32**, 1876 (1961).
10. Junqian Zhang, Bo Lu, Yicheng Song, and Xiang Ji, *Journal of Power Sources*, **209**, 220 (2012).
11. Y.-T. Cheng and M. W. Verbrugge, *Journal of Power Sources*, **190**, 453 (2009).
12. Rutooj Deshpande, Yang-Tse Cheng, and Mark W. Verbrugge, *Journal of Power Sources*, **195**, 5081 (2010).
13. Y. Song, B. Lu, X. Ji, and J. Zhang, *Journal of the Electrochemical Society*, **159**, A2060 (2012).
14. J. Li, Q. Fang, F. Liu, and Y. Liu, *Journal of Power Sources*, **272**, 121 (2014).
15. T. Zhang, Z. Guo, Y. Wang, and J. Zhu, *Journal of Applied Physics*, **115**, 083504 (2014).
16. John Christensen and John Newman, *J. Solid State Electrochem*, **10**, 293 (2006).
17. Xiangchun Zhang, Wei Shyy, and Ann Marie Sastry, *Journal of The Electrochemical Society*, **154**, A910 (2007).
18. William H. Woodford, Yet-Ming Chiang, and W. Craig Carter, *Journal of The Electrochemical Society*, **157**, A1052 (2010).
19. Pallab Barai and Partha P. Mukherjee, *Journal of The Electrochemical Society*, **163**, A1120 (2016).
20. K. Zhao, M. Pharr, S. Cai, J. J. Vlassak, and Z. Suo, *Journal of the American Ceramic Society*, **94**, s226 (2011).
21. Z. Cui, F. Gao, and J. Qu, *Journal of the Mechanics and Physics of Solids*, **61**, 293 (2013).
22. Yong Li, Kai Zhang, Bailin Zheng a, and Fuqian Yang, *Journal of Power Sources*, **319**, 168 (2016).
23. X. T. Duan, W. J. Jiang, Y. L. Zou, W. X. Lei, and Z. S. Ma, *Journal of Materials Science*, **53**, 10987 (2018).
24. Li Weng, Jianqiu Zhoua, and Rui Cai, *International Journal of Mechanical Sciences*, **141**, 245 (2018).
25. P. Y. Hou, L. Q. Zhang, and X. P. Gao, *Journal of Materials Chemistry A*, **2**, 17130 (2014).
26. W. Liu, P. Oh, X. Liu, M.-J. Lee, W. Cho, S. Chae, Y. Kim, and J. Cho, *Angew. Chem. Int. Ed*, **54**, 4440 (2015).
27. Q. Wei, X. Wang, X. Yang, B. Ju, B. Hu, H. Shu, W. Wen, M. Zhou, Y. Song, H. Wu, and H. Hu, *Journal of Materials Chemistry A*, **1**, 4010 (2013).
28. GMK. Jr, I. Belharouak, H. Deng, Y. K. Sun, and K. Amine, *Chemistry of Materials*, **23**, 1954 (2011).
29. Y. Li, K. Zhang, and B. Zheng, *Journal of the Electrochemical Society*, **162**, A223 (2015).
30. Z. Cui, F. Gao, and J. Qu, *Journal of the Mechanics and Physics of Solids*, **60**, 1280 (2012).
31. Yaotian Zhong, Yulan Liu, and B Wang, *AIP Advances*, **7**, 075115 (2017).
32. F. C. Larché and J. W. Cahn, *Acta Metallurgica*, **33**, 331 (1985).
33. Y. Li, K. Zhang, and B. Zheng, *Solid State Ionics*, **283**, 103 (2015).
34. Kai Zhang, Yong Li, and Bailin Zheng, *Journal of Applied Physics*, **118**, 105102 (2015).
35. R. A. Huggins and W. D. Nix, *Ionics*, **6**, 57 (2000).
36. Tanmay K. Bhandakkar and Huajian Gao, *International Journal of Solids and Structures*, **40**: 1424 (2010).